# Vibration of the weapon system on an unmanned ground vehicle during movement

*Viet Dung* Bui[a], *Martin* Macko[b], *Ba Ngoc* Dang[c], *Huu Nguyen* Pham[d]

[a] University of Defence, Faculty of Military Technology, Department of Weapons and Ammunition, Brno, Czech Republic,
e-mail: vietdung.bui@unob.cz,
ORCID iD: https://orcid.org/0009-0004-9752-9054

[b] University of Defence, Faculty of Military Technology, Department of Weapons and Ammunition, Brno, Czech Republic,
e-mail: martin.macko@unob.cz, **corresponding author**,
ORCID iD: https://orcid.org/0000-0002-3896-0803

[c] University of Defence, Faculty of Military Technology, Department of Weapons and Ammunition, Brno, Czech Republic,
e-mail: bangoc.dang@unob.cz,
ORCID iD: https://orcid.org/0009-0006-0481-4572

[d] Tran Dai Nghia University, Faculty of Ammunition, Department of Explosives and Ballistics, Hochiminh, Socialist Republic of Vietnam,
e-mail: huunguyenvhp@gmail.com,
ORCID iD: https://orcid.org/0009-0004-9615-9426

https://doi.org/10.5937/vojtehg74-61289

FIELD: mechanical engineering
ARTICLE TYPE: original scientific paper

*Abstract:*

*Introduction/purpose: The article presents a mathematical model of the vibration of a weapon mount on a small unmanned ground vehicle (UGV) with a total weight of up to 70 kg, including the weapon. The design of these small vehicles is similar to that of larger combat vehicles: a mount is placed on a wheeled or tracked chassis, allowing the weapon to be elevated and azimuthally adjusted, and if it allows firing while moving, the angular position of the barrel is affected by chassis vibration and should be stabilized. The vibration of the chassis and parts of the weapon mount is not desirable, and the results of vibration simulation allow for the design of a solution that will eliminate it.*

*Methods: A system of differential equations describing the vibrations of the weapon system and a system of equations describing the motion of the vehicle over terrain were created. Subsequently, the vibrations were simulated in Matlab-Simulink software. Further testing was carried out to*

*measure the deviation of the camera axis from the center of the target. The results of the experiment were compared with the results of the simulation.*

*Results: The research results indicate that the vibration of the weapon system on unmanned ground vehicles depends on many factors, such as the road surface profile, tire properties, suspension system, and overall dimensions, layout, and weight of components. The experimental results of camera stability measurements during target tracking correspond to the simulation results in Matlab-Simulink software.*

*Conclusion: The system of mathematical differential equations of an unmanned ground vehicle, together with the road profile model, describes the factors affecting the vibration of the weapon system during vehicle movement. Mathematical models allow for parameter changes and thus enable simulation of changes in the angular position of the barrel for other input conditions.*

*Key words: unmanned ground vehicle, weapon system, stabilization, vibration analysis.*

## Introduction

Unmanned Ground Vehicles (UGVs) are vehicles that move on the ground without human presence on board. These vehicles are equipped with weapon systems used to destroy targets such as enemy forces, fortifications on land and water, as well as low-altitude aerial vehicles, etc. Using UGVs helps avoid human losses, dangers on the battlefield, reduce financial losses and at the same time increase combat effectiveness in modern warfare.

The vehicle has a sensor system to observe the environment. These sensors are electronic devices used to measure the angle of deviation of the barrel in range and direction relative to the target, based on changes in physical processes (pressure, temperature, sound, light, etc.) from the surrounding environment emitted by the target and converted into electrical signals used to send information to the controllers. The controller sends control signals to the servo motors. The servo motor is a closed-loop transmission and feedback system used to create control torque quickly and accurately. The UGV uses two servo motors, one motor to control the azimuth angle and one to control the direction of the barrel. The servo motors control the position, regulate the speed accurately, and adjust the torque appropriately to direct the barrel to the target.

There have been many studies on the mathematical modeling and simulation of weapon system vibrations on main battle tanks, however, these studies have not yet specifically calculated the influence of the road surface profile when the vehicle is in motion, nor have they sufficiently

examined unmanned vehicles. Abdeselem et al. (2024) developed a mathematical model and simulated the suspension system of a half vehicle in the roll plane with four degrees of freedom. The study focused on the influence of the suspension system on vehicle performance characteristics such as ride comfort, road holding, and working space. The study by Karayumak (2011) was conducted under experimental conditions at Aberdeen Proving Ground (APG), focusing on a main battle tank moving on a bumpy road surface and during turning maneuvers. The experimental data measured on the computer are the input factors for the simulation problems. Ambarish et al. (2017) focused on developing a mathematical model of the elevation dynamics of a tracked vehicle using a half-vehicle model. Differential equations were developed for the weapon system using the state-space approach, simulating the elevation dynamic on the half-vehicle body. The elevation dynamic model of the weapon system includes three degrees of freedom, generated from the rotational dynamics of the drive, breech section and muzzle section. Then, backstepping, LQR (Linear Quadratic Regulator) and PID control techniques were integrated into the state space matrix for the coupled dynamic model, in which the control parameters were determined through different iterations. David (2001), Hallbeck (2021) developed mathematical equations of motion for the weapon system on a tracked vehicle with a suspension system, based on rotation matrices. The above authors have measured and calculated the actual model and then simulated the vibration system. The unmanned vehicle is a combination of a suspension system, azimuth drive, elevation drive and firing system. These are the parameters that determine the stability of the barrel. The suspension system of the vehicle body helps the vehicle move smoothly, reducing vibrations on uneven terrain. The azimuth drive has the effect of transmitting the rotation of the turret in the horizontal plane, while the elevation drive rotates the barrel in the vertical plane with the help of an electric motor driving the reduction gear. The barrel rotates in the vertical plane created by the electric motor connected to the turret ring, as described by Hallbeck (2021) and Cagil (2016).

This study develops a system of mathematical equations of a vehicle with seven degrees of freedom, combined with a six-degree-of-freedom azimuth dynamics model and five-degree-of-freedom elevation dynamics model. In the experimental section, this paper employs the DJI RoboMaster S1 platform to measure the deviation of the camera center during a human target-tracking task. A gimbal-mounted camera is used to continuously orient the lens toward the moving target. The tracking process is conducted in a real-world environment, with the target being a person moving freely in various directions and at different speeds. The

image coordinates of the target's center are continuously recorded using an object detection algorithm and compared with the center coordinates of the camera frame. The deviation is quantified as the Euclidean distance between the target's center and the frame center and it is collected across multiple time samples for analysis. Experimental results show that the deviation increases significantly when the target moves rapidly or changes direction abruptly, particularly during moments when the gimbal system has not yet fully compensated. The collected data play an important role in evaluating the gimbal controller's performance and optimizing the tracking algorithm to enhance system stability and accuracy. Moreover, these experimental results can also be applied to assess the vibrations of a weapon system mounted on an unmanned ground vehicle, under the influence of terrain conditions, vehicle speed, direction of motion, and dynamic torque disturbances from the actuator.

## Mathematical model

### *Mathematical model of the unmanned vehicle*

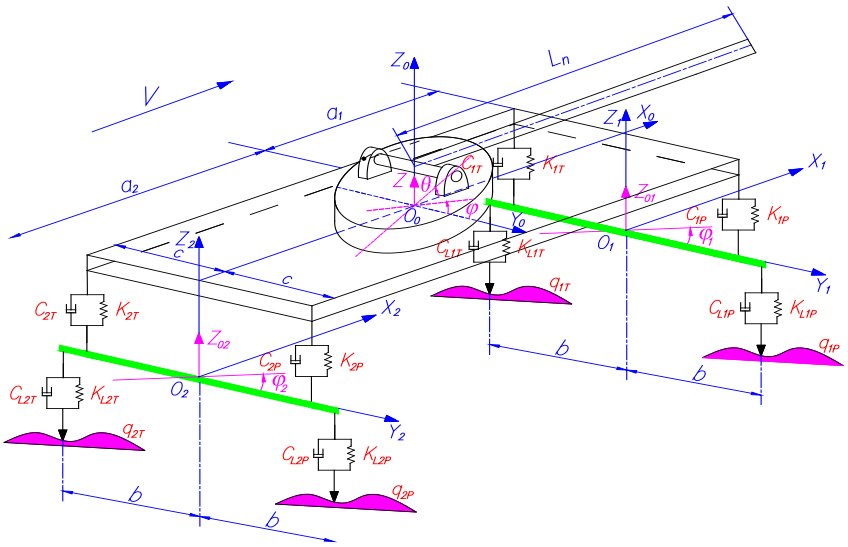


*Figure 1 - Unmanned vehicle model*

The research model includes the following elements: vehicle body, turret, barrel, front axle, and rear axle (Bui et al, 2024).

The model uses three coordinate systems. The $O_0X_0Y_0Z_0$ coordinate system is located at the center of gravity of the vehicle body, the $O_1X_1Y_1Z_1$

coordinate system is located at the center of gravity of the front axle, whereas the $O_2X_2Y_2Z_2$ coordinate system is located at the center of gravity of the rear axle.

Symbols: $q_{1T}$, $q_{1P}$, $q_{2T}$, $q_{2P}$ denote the roughness of the road surface at the contact points with the front and rear tires on the left and right sides.

$C_{L1T}$, $K_{L1T}$, $C_{L1P}$, $K_{L1P}$, $C_{L2T}$, $K_{L2T}$, $C_{L2P}$, $K_{L2P}$ denote the damping coefficient and elasticity coefficient of the front and rear tires on the left and right sides.

$C_{1T}$, $K_{1T}$, $C_{1P}$, $K_{1P}$, $C_{2T}$, $K_{2T}$, $C_{2P}$, $K_{2P}$ denote the coefficient and elasticity coefficient of the front and rear suspension on the left and right sides.

$a_1$, $a_2$ denote the distance from the center of gravity of the vehicle body to the front axle and rear axle; $2b$ denotes the average distance between the right and left wheel tracks; $2c$ denotes the average distance between left and right suspension; $Z_{01}$, $\varphi_1$, $Z_{02}$, $\varphi_2$ denote the vertical displacement and roll angle of the front and rear axles; $Z_0$, $\varphi$, $\theta$ denote the vertical displacement, roll angle, pitch angle of the vehicle body; $L_n$ denotes the barrel length; $L=a_1+a_2$ denote the standard long; $V$ is the vehicle speed.

$F_{CL1T}, F_{KL1T}, F_{CL1P}, F_{KL1P}, F_{CL2T}, F_{KL2T}, F_{CL2P}, F_{KL2P}$ denote the damping and elastic force of the front and rear tires on the left and right.

$F_{C1T}, F_{K1T}, F_{C1P}, F_{K1P}, F_{C2T}, F_{K2T}, F_{C2P}, F_{K2P}$ denote the damping and elastic force of the front and rear suspension on the left and right.

### *Road surface function equation*

The article uses the Inverse Fourier Transform method based on ISO 8608:2016 to represent the road surface profile over time.

The height of the road surface profile over time is determined by the following formula (Liangkuan et al, 2023; Bui et al, 2025):

$$q_{(t)} = \sum_{i=1}^{n} \sqrt{4 S_q \Delta\Omega \cos\left(\Omega_i t + \gamma_i\right)} \tag{1}$$

where: $q_{(t)}$ is the height of the road surface bump, $S_q$ is the power spectral density of the road surface bump according to ISO 8608:2016, $\Omega_i$ is the spatial frequency of the road surface profile, $\Delta\Omega$ is the point distance divided by spatial frequency calculated according to the simulation path length L, $\gamma_i$ is the initial phase, which is random and usually chosen according to a uniform distribution in the interval [0,2π], $n$ is the upper limit of the sum, representing the number of components taken to approximate the amplitude of the rough pavement surface. It indicates the

number of spatial frequencies considered when calculating the pavement profile. The larger the value of $n$, the more accurate the model is in representing the actual pavement surface.

The power spectrum of the pavement is determined by the following formula (Liangkuan et al, 2023):

$$S_q(\Omega) = \begin{cases} S_{q(\Omega_0)} \left( \dfrac{\Omega}{\Omega_0} \right)^{-w} & \Omega_1 \le \Omega \le \Omega_2 \\ 0 & \Omega < \Omega_1;\ \Omega > \Omega_2 \end{cases} \quad (2)$$

where: $\Omega_1, \Omega_2$ are spatial frequency limits determined from the time-frequency range $f_1, f_2$ and the vehicle's speed $V$ in the direction $X$.

$$\Omega_1 = f_1 / V; \qquad \Omega_2 = f_2 / V \quad (3)$$

$\Omega_0$ is the reference spatial frequency, with $\Omega_0 = 0{,}1\ m^{-1}$, $w$ is the exponent index (usually $w = 2$), and $S_{q(\Omega_0)}$ is determined based on the ISO 8608:2016 standard presented in Table 1.

*Table 1 - Power spectrum density by road surface levels*

| Road surface levels | $S_{q(\Omega_0)}(10^{-6} m^2/m^{-1})$ with $\Omega_0$ = 0.1 ($m^{-1}$) | | | $S_{q(\Omega)}(10^{-6} m^2/m^{-1})$ with 0.011$m^{-1}$≤ Ω ≤ 2.83$m^{-1}$ | | |
|---|---|---|---|---|---|---|
| | Lower bound | Average | Upper bound | Lower bound | Average | Upper bound |
| A | 8 | 16 | 31 | 2.69 | 3.81 | 5.38 |
| B | 32 | 64 | 128 | 5.38 | 7.61 | 10.77 |
| C | 128 | 256 | 512 | 10.77 | 15.23 | 21.53 |
| D | 512 | 1024 | 2048 | 21.53 | 30.45 | 43.06 |
| E | 2048 | 4096 | 8192 | 43.06 | 60.90 | 86.13 |
| F | 8192 | 16284 | 32768 | 86.13 | 121.80 | 172.26 |
| G | 32768 | 65536 | 131072 | 172.26 | 243.61 | 344.52 |
| H | 131072 | 262144 | 524288 | 344.52 | 487.22 | 689.04 |

## The mathematical equations of the vehicle body

The mathematical model was developed in studies by Bui et al. (2024, 2025), based on previous research by Chen et al. (2012), Yin et al. (2023) and Kim et al. (2024).

$$
\begin{aligned}
&m_1.Z''_{01} = -F_{CL1T} - F_{KL1T} - F_{CL1P} - F_{KL1P} + F_{C1T} + F_{K1T} + F_{C1P} + F_{K1P} \\
&J_{m1}.\varphi''_1 = b\left[\left(F_{CL1T} + F_{KL1T}\right) - \left(F_{CL1P} + F_{KL1P}\right)\right] + c\left[\left(F_{C1P} + F_{K1P}\right) - \left(F_{C1T} + F_{K1T}\right)\right] \\
&m_2 Z''_{02} = -F_{CL2T} - F_{KL2T} - F_{CL2P} - F_{KL2P} + F_{C2T} + F_{K2T} + F_{C2P} + F_{K2P} \\
&J_{m2}.\varphi''_2 = b\left[\left(F_{CL2T} + F_{KL2T}\right) - \left(F_{CL2P} + F_{KL2P}\right)\right] + c\left[\left(F_{C2P} + F_{K2P}\right) - \left(F_{C2T} + F_{K2T}\right)\right] \\
&(M_k + \mathrm{M}_n + \mathrm{M}_t)Z'' = -F_{C1T} - F_{K1T} - F_{C1P} - F_{K1P} - F_{C2T} - F_{K2T} - F_{C2P} - F_{K2P} \\
&(J_{xk} + \mathrm{J}_{xn} + \mathrm{J}_{xt})\varphi'' = c\left[\left(F_{C1T} + F_{K1T}\right) - \left(F_{C1P} + F_{K1P}\right)\right] + c\left[\left(F_{C2T} + F_{K2T}\right) - \left(F_{C2P} + F_{K2P}\right)\right] \\
&(J_{yk} + \mathrm{J}_{yn} + \mathrm{J}_{yt})\theta'' = -a_1\left[\left(F_{C1P} + F_{K1P}\right) + \left(F_{C1T} + F_{K1T}\right)\right] + a_2\left[\left(F_{C2P} + F_{K2P}\right) + \left(F_{C2T} + F_{K2T}\right)\right]
\end{aligned}
\tag{4}
$$

## System of equations for elevation dynamics

The kinematic dimensions and diagrams of the forces acting on the elevation dynamics block are given in Figure 2 by Banerjee et al. (2016, 2018), Ambarish et al. (2017), Jitesh (2018) and Bui et al. (2025).

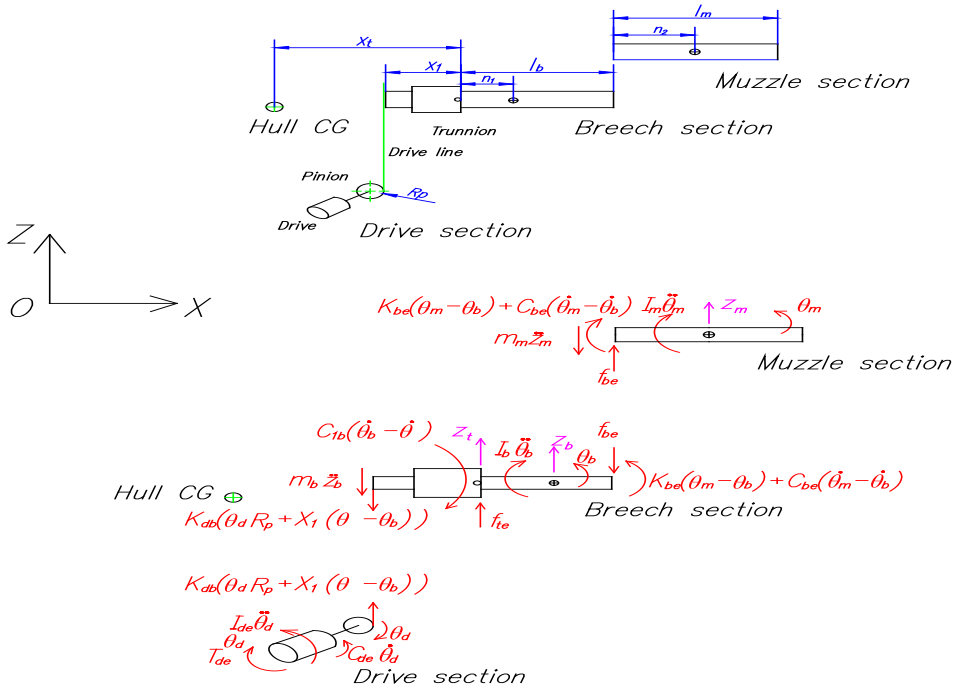


*Figure 2 - Diagram of the forces acting on the elevation dynamics*

The following symbols are used in the diagram:

$\theta, \theta_d, \theta_b, \theta_m$ represent the roll angle of the vehicle body, the rotation angle of the drive, the rotation angle of the breech section and the muzzle section in the vertical plane;

$T_{de}, I_{de}, I_b, I_m$ are the torsional torque, the mass moment of inertia of the drive, the mass moment of inertia of the breech section and the muzzle section;

$K_{db}, K_{be}$ are the driveline stiffness of rack and pinion arrangement for the elevation and torsional stiffness of the breech section with the muzzle section;

$C_{1b}, C_{de}, C_{be}$ demote the torsional viscous damping coefficient of the trunnion hinge about the $OY$ axis, the torsional viscous damping in the elevation drive, the torsional viscous damping at the connection interface between the breech section and the muzzle section about the $OY$ axis;

$m_b, m_m$ are the mass of the breech section and the muzzle section;

$z_b, z_m$ are the vertical displacement at the center of gravity of the breech section and the muzzle section;

$f_{te}, f_{be}$ denote the reaction force acting at the pivot joint, the reaction force acting at the junction point between the breech section and the muzzle section;

$X_t$ is the distance from the center of gravity of the vehicle body to the axis of rotation of the barrel in the vertical plane;

$X_1$ is the distance of the transmission line to the axis of rotation;

$n_1$ is the distance from the axis of rotation to the center of gravity of the breech section;

$l_b$ is the distance from the axis of rotation to the point of junction between the breech section and the muzzle section;

$n_2$ is the distance from the point of junction of the breech section and the muzzle section to the center of gravity of the muzzle section;

$l_m$ is the length of the muzzle section.

The mathematical model was developed by Bui et al. (2025).

$$
\begin{aligned}
I_{de}\theta''_d &= T_{de} - C_{de}\theta'_d - K_{db}\left[\theta_d R_p + X_1(\theta-\theta_b)\right]R_p \\
I_b\theta''_b &= -C_{1b}(\theta'_d-\theta') - f_{be}(l_b-n_1) - f_{te}n_1 + K_{be}(\theta_m-\theta_b) + \\
&\quad + C_{be}(\theta'_m-\theta'_b) + K_{db}\left[\theta_d R_p + X_1(\theta-\theta_b)\right](X_1+n_1) \\
m_b z''_b &= f_{te} - K_{db}\left[\theta_d R_p + X_1(\theta-\theta_b)\right] - f_{be} \\
I_m\theta''_m &= -f_{be}n_2 - K_{be}(\theta_m-\theta_b) - C_{be}(\theta'_m-\theta'_b) \\
m_m z''_m &= f_{be}
\end{aligned}
\tag{5}
$$

## *System of equations for azimuth dynamics*

The force diagram acting on the azimuth dynamics and the symbols used are given in Figure 3, as in Ambarish et al. (2017) and Jitesh (2018).

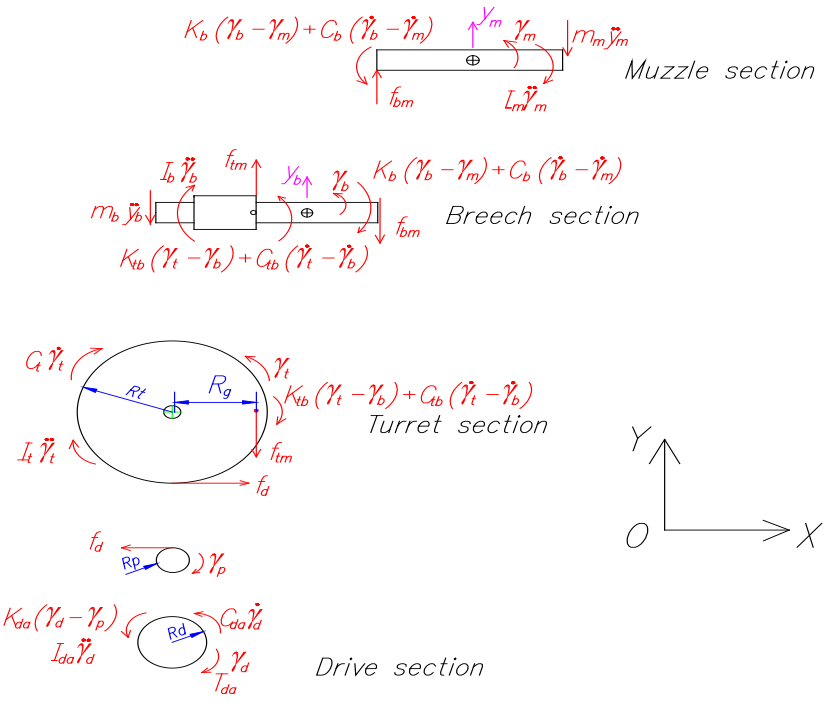


*Figure 3 - Diagram of the forces acting on the azimuth dynamics*

The symbols used in the figure are as follows:

$\varphi, \gamma_d, \gamma_t, \gamma_b, \gamma_m$ are the pitch angle of the vehicle body, the rotation angle of the drive, the rotation angle of the turret gear ring, the rotation angle of the breech section and the muzzle section in the horizontal plane;

$T_{da}, I_{da}, I_t, I_b, I_m$ are the torsional torque, the mass moment of inertia of the drive, the mass moment of inertia of the turret, the mass moment of inertia of the breech section and the muzzle section;

$K_{da}$ is the torsional stiffness of the azimuth drive, $K_{tb}$ is the torsional stiffness about the $OZ$ axis, at the trunnion interface, connecting the breech section and turret, $K_b$ is the torsional stiffness about the $OZ$ axis at the connection interface between the breech and the muzzle sections;

$C_{da}$ is the torsional viscous damping coefficient in the azimuth drive, $C_{tb}$ is the torsional viscous damping about the $OZ$ axis, at the trunnion interface, connecting the gun breech section and the turret;

$C_b$ is the torsional viscous damping about the $OZ$ axis, at the connection interface between the breech and the muzzle sections;

$y_b, y_m$ are the displacements at the center of gravity of the breech section and the muzzle section, $f_d, f_{tm}, f_{bm}$ are the reaction force at the point of contact between the pinion and the turret ring gear, measured along the $OZ$ direction and the turret roller gear, the reaction force between the turret with the breech and reaction force the breech point of contact between the breech section and the muzzle section;

$R_d, R_p, R_t, R_g$ are the radius of the engine gear, the transmission gear, the turret gear ring and the distance from the center of gravity of the turret to the axis of rotation.

The system of differential equations for azimuth dynamic consists of six equations with six unknowns $\gamma_d, \gamma_t, \gamma_b, y_b, \gamma_m, y_m$, as in Bui et al. (2025).

$$
\begin{aligned}
&I_{da}\gamma''_d = T_{da} - K_{da}\left(\gamma_d - \frac{R_t\gamma_t}{R_p}\right) - C_{da}\gamma'_d \\
&I_t\gamma''_t = K_{da}R_t\left(\frac{R_p\gamma_d - R_t\gamma_t}{R_p^2}\right) - C_t\gamma'_t - K_{tb}\left(\gamma_t - \gamma_b\right) - C_{tb}\left(\gamma'_t - \gamma'_b\right) - R_g\left(m_b y''_b + m_m y''_m\right) \\
&I_b\gamma''_b = -\left(m_b y''_b + m_m y''_m\right)n_1 - m_m y''_m\left(l_b - n_1\right) + K_{tb}\left(\gamma_t - \gamma_b\right) + C_{tb}\left(\gamma'_t - \gamma'_b\right) + K_b\left(\gamma_m - \gamma_b\right) + C_b\left(\gamma'_m - \gamma'_b\right) \\
&y_b = X_t\gamma_t + n_1\gamma_b \\
&I_m\gamma''_m = K_b\left(\gamma_b - \gamma_m\right) + C_b\left(\gamma'_b - \gamma'_m\right) + n_2 m_m y''_m \\
&y_m = X_t\gamma_t + l_b\gamma_b + n_2\gamma_m
\end{aligned}
\tag{6}
$$

Because the barrel and the turret system are mounted on the vehicle body and are directly affected by its motion, the elevation dynamics are

coupled with the vehicle body's roll and pitch angles through an integration equation.

$$z_b = Z + \theta X_t - X_t \varphi \sin\gamma_t + \theta_b n_1 - n_1 \varphi \sin\gamma_t$$
$$z_m = Z + \theta X_t - X_t \varphi \sin\gamma_t + \theta_m n_2 + \theta_b l_b - (l_b + n_2)\varphi \sin\gamma_t \quad (7)$$

# Simulation results

## *Simulation input parameters*

The input parameters for simulating vehicle vibration as well as the azimuth and elevation motions are provided in Table 2 and Table 3. The values used in the simulation are based on Ambarish et al. (2017), Banerjee (2018), Bui et al. (2024, 2025).

*Table 2 - Parameters for simulating the system of vibration differential equations*

| Quantities | Values | Quantities | Values | Quantities | Values |
|---|---|---|---|---|---|
| Front axle | | | | | |
| $m_1$ | 210 kg | $K_{L1T}$ | 800000 N/m | $C_{L1T}$ | 2000 N.s/m |
| $b$ | 0.75 m | $K_{L1P}$ | 800000 N/m | $C_{L1P}$ | 2000 N.s/m |
| Rear axle | | | | | |
| $m_2$ | 260 kg | $K_{L2T}$ | 800000 N/m | $C_{L2T}$ | 2000 N.s/m |
| $b$ | 0.75 m | $K_{L2P}$ | 800000 N/m | $C_{L2P}$ | 2000 N.s/m |
| Vehicle body | | | | | |
| $M_k$ | 2480 kg | $K_{1T}$ | 180000 N/m | $K_{2T}$ | 180000 N/m |
| $a_1$ | 1.3 m | $K_{1P}$ | 180000 N/m | $K_{2P}$ | 180000 N/m |
| $a_2$ | 1.5 m | $C_{1T}$ | 9000 N.s/m | $C_{2T}$ | 9000 N.s/m |
| $c$ | 0.6 m | $C_{1P}$ | 9000 N.s/m | $C_{2P}$ | 9000 N.s/m |
| $J_{xk}$ | 4800 kg.m2 | $J_{yk}$ | 2000 kg.m2 | | |
| Turret and barrel | | | | | |
| $M_t$ | 1200 kg | $J_{yt}$ | 3800 kg.m2 | $J_{xt}$ | 3500 kg.m2 |
| $M_n$ | 500 kg | $J_{xn}$ | 600 kg.m2 | $J_{yn}$ | 450 kg.m2 |

*Table 3 - Parameters for elevation dynamics and azimuth dynamics*

| Quantities | Values | Quantities | Values | Quantities | Values |
|---|---|---|---|---|---|
| Parameters for elevation dynamics | | | | | |
| $I_{de}$ | 0.5 kg.m2 | $K_{db}$ | 3500 N/m | $C_{de}$ | 8000 N.m.s/rad |
| $I_b$ | 900 kg.m2 | $K_{be}$ | 1200 N.m/rad | $C_{be}$ | 500 N.m.s/rad |
| $I_m$ | 200 kg.m2 | $C_{1b}$ | 8000 N.m.s/rad | $m_b$ | 400 kg |
| $X_t$ | 0.3 m | $X_1$ | 0.15 m | $m_m$ | 120 kg |
| $n_1$ | 0.4 m | $l_b$ | 1.2 m | $n_2$ | 0.3 m |
| Parameters for azimuth dynamics | | | | | |
| $I_{da}$ | 25 kg.m2 | $R_t$ | 0.45 m | $C_{da}$ | 300 N.m.s/rad |
| $I_t$ | 2000 kg.m2 | $R_p$ | 0.06 m | $C_{tb}$ | 250 N.m.s/rad |
| $K_{da}$ | 400 N.m/rad | $K_{tb}$ | 300 N.m/rad | $C_b$ | 300 N.m.s/rad |
| $K_b$ | 350 N.m/rad | $C_t$ | 300 N.m.s/rad | $R_g$ | 0.3 m |

For the elevation and azimuth motions, small-amplitude torque inputs are applied to investigate the disturbances of the barrel induced by the servo motors. The input torque profiles for the elevation and azimuth axes are illustrated in Figure 4, as shown by Jitesh (2018).

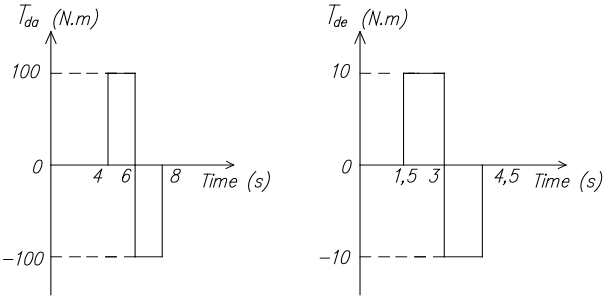


*Figure 4 - Applied torque inputs to the servo motors for azimuth and elevation angle control*

## *Road surface profile simulation*

The paper simulates different road surface profiles on the left and right sides to generate lateral vibrations for the barrel. The simulation uses a

level B road surface profile, with a speed of 8.33 m/s, $S_{q(\Omega_0)} = 64 \times 10^{-6}\, m^2 / m^{-1}$ and a simulation duration of 20 seconds. The results of the road surface profile simulation are shown in Figure 5 and Figure 6.

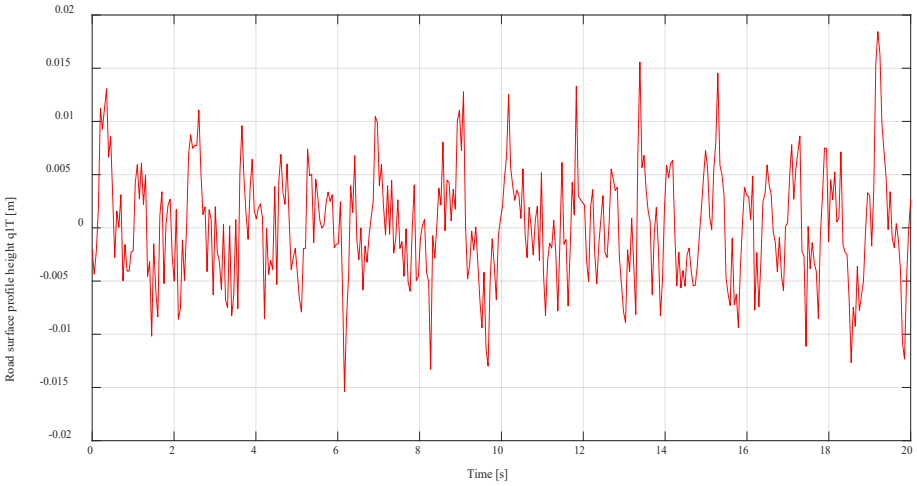


*Figure 5 - Road surface profile height on the left side $q_T$*

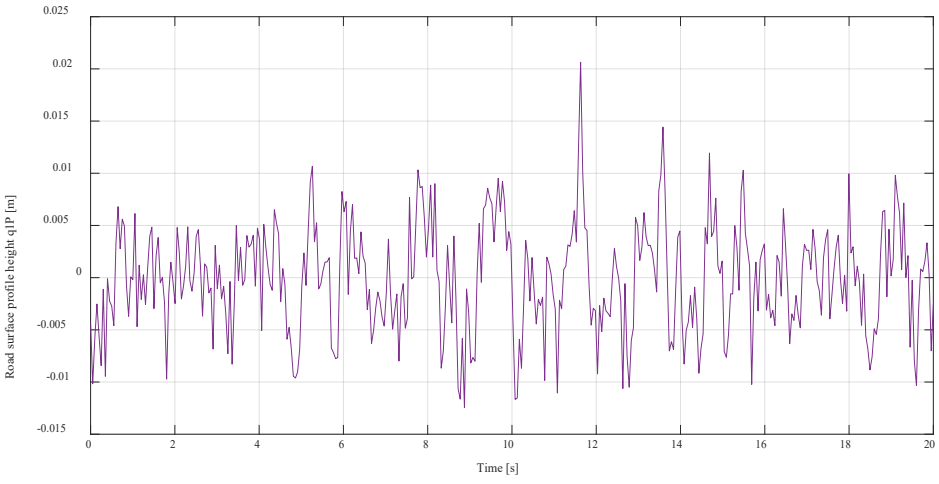


*Figure 6 - Road surface profile height on the right side $q_P$*

## *Simulation of longitudinal and angular vibrations of the barrel*

### *Vibrations in the vertical plane*

The simulation results shown in Figure 7 and Figure 8 represent the longitudinal and angular vibrations of the barrel in the vertical plane.

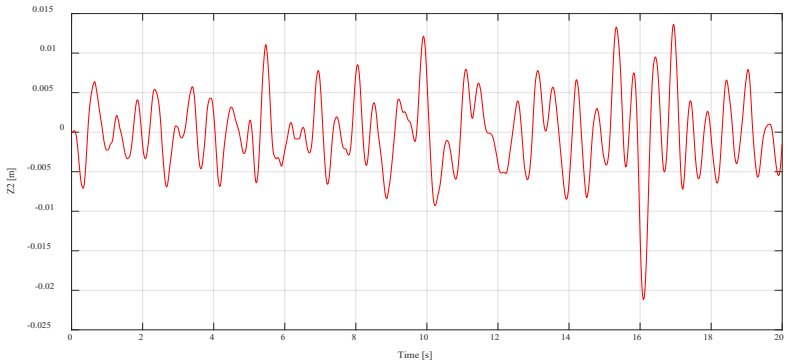


*Figure 7 - Graph of the longitudinal vibration amplitude of the barrel in the vertical plane*

From the graph shown in Figure 7, the vibration amplitude of the barrel ranges from $-0.021 \div 0.014\ m$, indicating that the barrel operates within a small amplitude with high-frequency vibrations, repeating several cycles per second. However, at approximately 16.1s, the vibration amplitude suddenly decreases, reaching a maximum value of about -0.021 m. Following this, the amplitude gradually decreases and returns to the small vibration level initially observed.

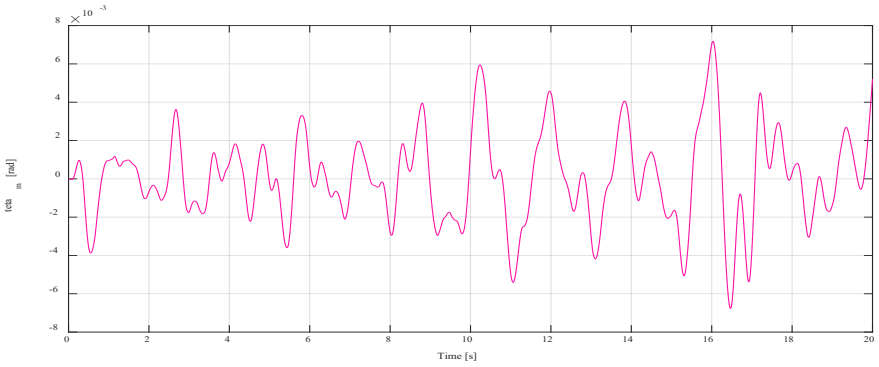


*Figure 8 - Angular vibration amplitude of the barrel in the vertical plane*

The angular vibration amplitude remains within the range of $-6.5\times10^{-3} \div 7.2\times10^{-3}\ rad$. The amplitude is not entirely uniform but shows slight variations over time, with some segments exhibiting higher amplitudes-particularly in the interval from $15 \div 16.5\ s$, where the amplitude reaches nearly $7.2\times10^{-3}\ rad$.

### *Vibrations in the horizontal plane*

The results of the longitudinal and angular vibrations of the barrel in the horizontal plane are shown in Figure 9 and Figure 10.

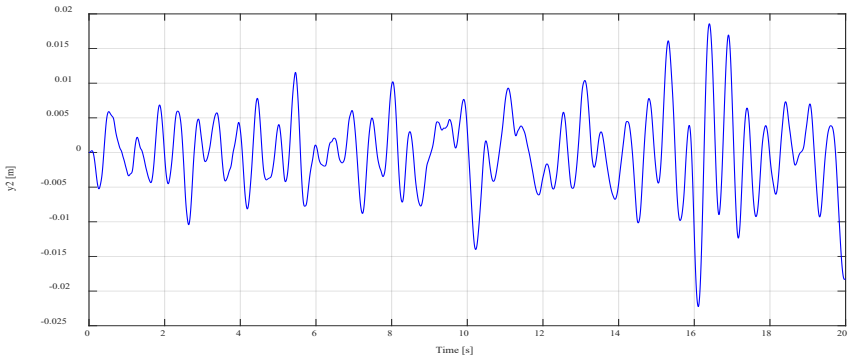


*Figure 9 - Longitudinal vibration amplitude of the barrel in the horizontal plane*

The graph can be observed that the vibration amplitude remains within a certain range around the equilibrium position.

These large amplitudes occur irregularly, suggesting the presence of abnormal external excitation forces. After each spike, the vibrations tend to decrease back to smaller amplitudes, though they do not fully return to the original steady-state condition.

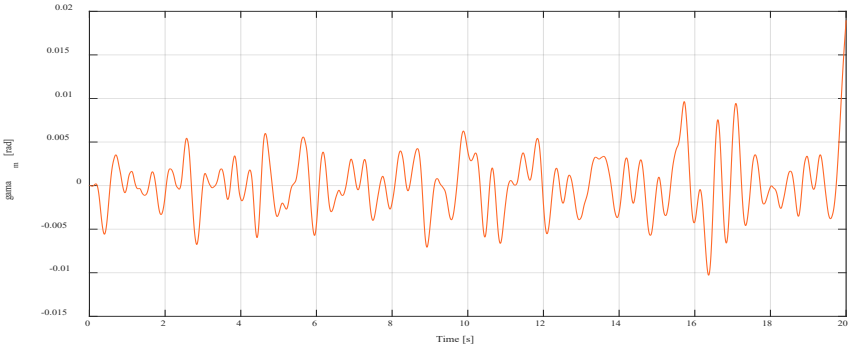


*Figure 10 - Angular vibration amplitude of the barrel in the horizontal plane*

In the range of 0-15 s, the vibrations of the gun barrel are relatively stable with small amplitudes, and the barrel does not deviate significantly from the equilibrium position. However, the sudden increase in amplitude at the end of the graph indicates that the system may encounter stability issues when subjected to large disturbances from road conditions.

The simulation results for the vibrations of the gun barrel in both the vertical and horizontal planes show a common characteristic: the vibration frequency is lower than the excitation frequency from the road. This can be explained by the damping coefficients and the spring constants of the suspension system and wheels. These factors help reduce the vibrations, contributing to greater stability of the gun barrel during movement and when the control motors are active.

## Experimental measurement of barrel vibrations on the DJI RoboMaster S1

### *Technical specifications of the DJI RoboMaster S1*

DJI RoboMaster S1 (Figure 11) is an intelligent robot developed and manufactured by DJI, a company based in China. The S1 is not only a remote-controlled robot but also a powerful educational tool that introduces users-especially beginners-to programming, artificial intelligence (AI), and robotics through its smart features. The robot supports programming in both Scratch 3.0 and Python, making it suitable for learners at all levels.

DJI RoboMaster S1 is equipped with a two-axis gimbal system consisting of a gun barrel and turret. Mounted above the barrel is a camera used for target tracking. The gimbal component is relatively lightweight, allowing for agile and responsive movement.

*Figure 11 - DJI RoboMaster S1*

The technical specifications of the DJI RoboMaster S1 are provided in Table 4.

*Table 4 - Main parameters of DJI RoboMaster S1*

| Parameters | |
|---|---|
| *Size* | 0.32 × 0.24 × 0.270 m |
| *Weight* | ≈ 3.3 kg |
| *2-axis gimbal* | Vertical plane $-20 \div 35^0$. Horizontal plane $-235 \div 235^0$ |
| *Drivetrain* | Four Mecanum wheels (omnidirectional movement), each equipped with 12 angled rollers. |
| *Engine* | Brushless M3508I motors with integrated FOC ESC. |
| *Control system* | Central controller with a processor that supports Python and Scratch programming. |
| *Camera* | 1 FPV camera (120° wide-angle), 1080p resolution, supports machine vision. |
| *Movement speed* | Maximum: ≈ 3.5 m/s (forward), ≈ 1 m/s (sideways). |
| *Rotation speed* | ≈ 600°/s |
| *Simulation weapons* | Gel bead gun, with a safety limit; integrated with a collision detection system. |
| *Sensor* | 6 armor sensors, distance sensors, IMU, encoder |
| *Programming* | Supports Python 3.6, Scratch 3.0; has extended API |
| *Machine vision* | Road, sign, person, gesture, and other robot recognition. |
| *Connect* | Wi-Fi Direct, control via mobile app or computer |

## *Experiment on the DJI RoboMaster S1*

The paper implements a target tracking and locking mode at a specific position on the human body. When the person moves, the robot follows and controls the turret to track the predetermined position. The target tracking is carried out through the integrated camera and computer vision algorithms. The images captured by the camera are processed directly on the machine or sent to a computer/phone to run computer vision algorithms. Once the person's position is determined, either through the bounding box or pixel coordinates, the system can control the turret's (gimbal's) elevation angle to track the target and simultaneously command the robot to move in follow mode to maintain pursuit. This is achieved by using feedback signals from the vision system to adjust the rotation motors and Mecanum wheels.

The area of the target zone is shown in Figure 12. The robot follows the target at a fixed distance.

*Figure 12 - The target bounding box is the back of the person's body*

When the target moves to the right or left, the robot will change its direction (Figure 13 and Figure14) and the controller will rotate the turret to follow the target.

*Figure 13 - The target moves to the right*

Figure *14 - The target moves to the left*

When the robot moves on an uneven road or when the target accelerates and changes direction, it causes vibrations between the camera's center and the target's center. This phenomenon is seen as jittering in the camera in real life when tracking a moving object that continuously changes direction, as clearly shown in Figure 13. The paper records a video of the robot tracking the target, then uses the Python programming language and the VidStab library on the robot to stabilize the video, i.e., to reduce the shaking and jittering in the original video. As we know, a video is a series of continuous frames, and stabilizing the video is equivalent to stabilizing each individual frame. After obtaining the stabilized video, we can calculate the deviations of each frame in both the horizontal and vertical directions, with the unit being radian. The experiment was conducted to measure angular deviations in the horizontal and vertical directions using a video with a duration of 89 seconds. The

distance from the camera center to the target is 2 m. The results are shown in Figures 15 and 16.

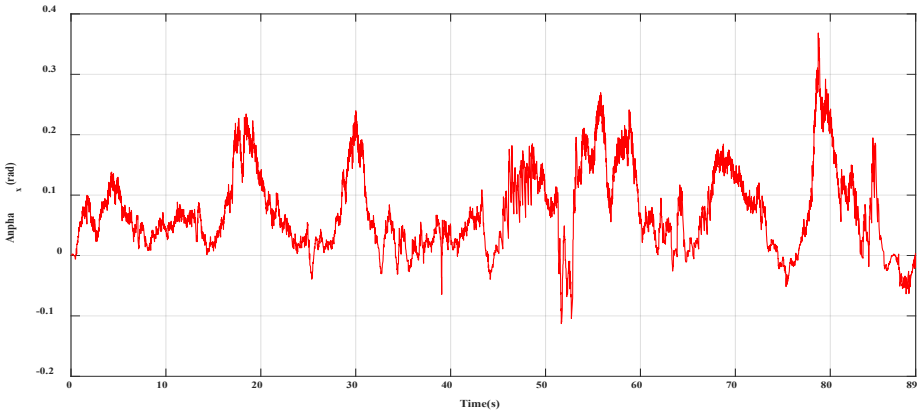


*Figure 15 - Angular deviation graph in the horizontal plane*

The graph illustrates that the angular deviation fluctuates continuously around a mean value of approximately 0.6 rad, with an amplitude ranging from –0.12 rad to +0.36 rad. During the oscillation process, numerous peaks and troughs can be observed, indicating significant dynamic phases-particularly evident in the time intervals of 18-20 s, 29-31 s, 51-59 s and 78-80 s. These variations reflect continuous changes in the relative position between the camera and the target, primarily caused by the target's directional shifts from left to right or vice versa, resulting in abrupt changes in oscillation amplitude. Additionally, the system is influenced by vehicle body vibrations, road surface conditions, and the response of the suspension system.

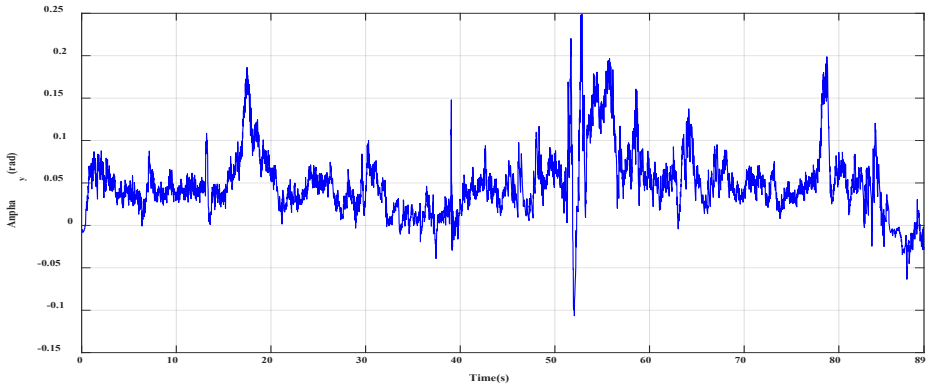


*Figure 16 - Angular deviation graph in the vertical plane*

The graph in Figure 16 shows that the oscillation amplitude remains relatively small and stable, as there is no significant change in the target's height. The amplitude ranges from -0.11 rad to 0.25 rad, with sudden increases observed during the intervals of 18-20 s, 51-56 s and 77-79 s.

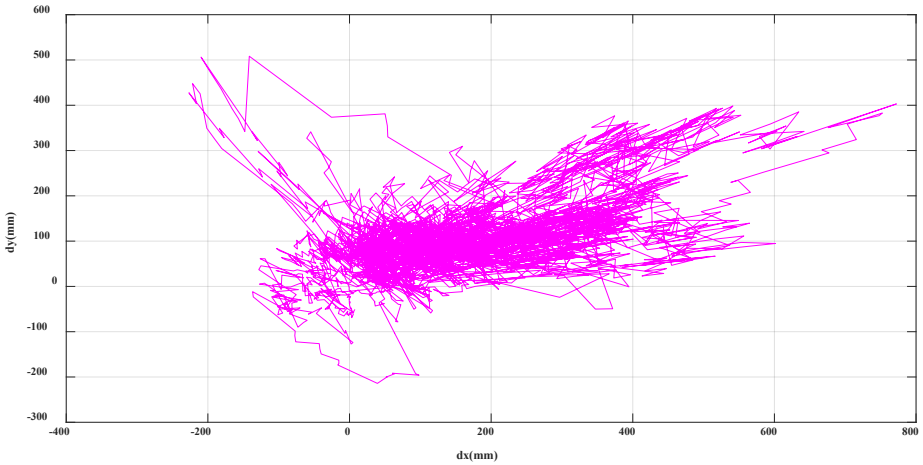


*Figure 17 - Barrel deflection position graph on coordinate plane*

The graph indicates that the deviation between the camera center and the target is greater in the horizontal direction than in the vertical direction. The horizontal deviation is concentrated within the range of 0-400 mm, while the vertical deviation remains within 0-200 mm. The above results accurately reflect the fact that when the barrel tracks the target, the deviation of the gun barrel depends greatly on the speed and direction of movement of the target.

## Conclusion

The experimental and simulation results exhibit similar vibration patterns, which can be interpreted as the vibration behavior of the cannon barrel on an autonomous vehicle. The curves in the simulation results are smooth due to the assumed input conditions and approximated outputs. In contrast, the experimental results reflect real-world conditions where the robot operates on actual terrain, involving directional changes and varying speeds. This distinction highlights the key differences between simulation and real-world testing outcomes.

From both simulation and the experiments conducted on the DJI RoboMaster S1, it is evident that road surface profiles, suspension system parameters, damping and spring characteristics, and torques generated

by control motors are critical factors contributing to cannon barrel vibrations during movement. The simulation model accurately captures the physical characteristics of the system, including terrain profile conditions, suspension stiffness, wheel dynamics, actuator behavior, and the physical properties of the cannon and turret system on the autonomous vehicle.

The barrel on an unmanned ground vehicle is strongly affected by road surface irregularities, directional changes, and torques from the control mechanism. When traversing uneven or rough terrain, the suspension system transmits vibrations to the vehicle body, which in turn propagates to the turret and barrel, producing forced vibrations with amplitudes and frequencies that vary based on terrain conditions. Additionally, during maneuvers such as turning, acceleration or deceleration, inertial torques are generated, leading to temporary misalignment and vibrations in the barrel.

Moreover, torque generated by the turret and elevation actuators, if not accurately controlled or if subject to latency, results in residual oscillations and deviations in aiming accuracy. The combination of these factors causes continuous misalignment in the aiming line, reducing the stability of the weapon system and potentially causing significant targeting errors, especially in scenarios that demand high precision in a short time. Therefore, compensating for these vibrations using sensors, controllers, and stabilization mechanisms plays a crucial role in maintaining targeting and firing accuracy under complex real-world conditions.

This study introduces a basic mathematical model and serves as a preparatory step for developing a comprehensive model to address the stability problem in subsequent studies.

## *References*

Abdeselem, B.B., Momir, M.D., Aleksandar, S.Đ., Sreten, R.P., Aleksandar, G.B. & Abdellah, B.F. 2024. Mathematical modeling and simulation of a half-vehicle suspension system in the roll plane. *Vojnotehnički glasnik/Military Technical Courier*, 72(1), pp.192-208. Available at: https://doi.org/10.5937/vojtehg72-47551.

Ambarish, J., Saayan, B. & Jebaraj, C. 2017. Development of mathematical models, simulating vibration control of tracked vehicle weapon dynamics. *Defence Science Journal*, 67(4), pp.465–475 [online]. Available at: https://www.researchgate.net/publication/318363890_Development_of_Mathematical_Models_Simulating_Vibration_Control_of_Tracked_Vehicle_Weapon_Dynamics [Accessed: 24 July 2025].

Banerjee, S., Balamurugan, V. & Krishnakumar, R. 2016. Ride comfort analysis of math ride dynamics model of full tracked vehicle with trailing arm

suspension. In: *International Conference on Vibration Problems 2015*, pp.1110–1118. Available at: https://doi.org/10.1016/j.proeng.2016.05.074.

Banerjee, S., Balamurugan, V. & Krishnakumar, R. 2018. Effect of integrated ride and cornering dynamics of a military vehicle on the weapon responses. *Proceedings of the Institution of Mechanical Engineers, Part K: Journal of Multi-body Dynamics*, 232(4). Available at: https://doi.org/10.1177/1464419318754647.

Bui, V.D., Martin, M., Zbynek, K., Tranh, D.D., Do, Q.V. & Pham, H.N. 2024. Mathematical model of unmanned ground vehicle. In: *International Conference QUAERE 2024*, Hradec Kralove, Czech Republic, 14, pp.765–771 [online]. Available at: http://www.vedeckekonference.cz/library/proceedings/quaere_2024.pdf [Accessed: 24 July 2025].

Bui, V.D., Martin, M., Tran, D.D., Martin, C. & Zbynek, K. 2025. Research on Vibrations of an Unmanned Vehicle on a Random Road Surface. In: *2025 International Conference on Military Technologies (ICMT)*, Brno, Czech Republic, 27-30 May 2025. Available at: https://doi.org/10.1109/ICMT65201.2025.11061271.

Bui, V.D., Martin, M., Miloš, M., Dejan, J. & Tran, D.D. 2025. Barrel Vibration of an Automatic Weapon on an Unmanned Vehicle. In: *2025 International Conference on Military Technologies (ICMT)*, Brno, Czech Republic, 27-30 May 2025. Available at: https://doi.org/10.1109/ICMT65201.2025.11061266.

Cagil, C. 2016. Dynamic modeling and analysis of gun turret elevation drive system. MSc thesis, Department of Mechanical Engineering, Middle East Technical University [online]. Available at: https://etd.lib.metu.edu.tr/upload/12620067/index.pdf [Accessed: 24 July 2025].

Chen, K., Zhang, M. & Tong, X. 2012. Vibration characteristic analysis of vehicle air suspension based on fuzzy control. In: *2nd International Conference on Electronic & Mechanical Engineering and Information Technology (EMEIT-2012)*, Paris, France, pp.2196–2199. Available at: https://doi.org/10.2991/emeit.2012.486.

David, J.P. 2001. Comparison of balance and out of balance main battle tank armaments. *Shock and Vibration*, 8(3–4), pp.167–174. Available at: https://doi.org/10.1155/2001/326219.

Hallbeck, V. 2021. System modelling and evaluation of main battle tank fire precision. MSc thesis, KTH Royal Institute of Technology, School of Engineering Sciences [online]. Available at: https://www.diva-portal.org/smash/get/diva2:1595629/FULLTEXT01.pdf [Accessed: 24 July 2025].

ISO. 2016. ISO 8608:2016 – Mechanical vibration – Road surface profiles – Reporting of measured data. International standard [online]. Available at: https://cdn.standards.iteh.ai/samples/71202/05b2151f255b44928f80acb897fc0c2c/ISO-8608-2016.pdf [Accessed: 24 July 2025].

Jitesh, S. 2018. Modelling and simulation of main battle tank to stabilize the weapon control system. In: *International Conference on Advances in Design, Materials, Manufacturing and Surface Engineering for Mobility*. Available at: https://doi.org/10.4271/2018-28-0078.

Kim, Y.J., Sohn, Y., Chang, S., Choi, S.B. & Oh, J.S. 2024. Vibration control of car body and wheel motions for in-wheel motor vehicles using road type classification. *Actuators*, 13(2). Available at: https://doi.org/10.3390/act13020080.

Liangkuan, W., Xu, T., Ji, F. & Cheng, H. 2023. Prediction of firing accuracy of self-propelled antiaircraft gun in marching fire based on GA-BP neural network. In: *International Conference on Defence Technology (2022 ICDT), IOP Conference Series: Journal of Physics: Conference Series*, 2478, 092007. Available at: https://doi.org/10.1088/1742-6596/2478/9/092007.

Yin, Z., Su, R. & Ma, X. 2023. Dynamic responses of 8-DoF vehicle with active suspension: Fuzzy-PID control. *World Electric Vehicle Journal*, 14(9), pp.1–23. Available at: https://doi.org/10.3390/wevj14090249.

---

Vibracije sistema naoružanja na besposadnom kopnenom vozilu tokom kretanja

*Viet Dung* Bui[a], *Martin* Macko[a], **autor za prepisku**, *Ba Ngoc Dang*[a], *Huu Nguyen* Pham[b]

[a] University of Defence, Faculty of Military Technology, Department of Weapons and Ammunition, Brno, Czech Republic,

[b] Tran Dai Nghia University, Faculty of Ammunition, Department of Explosives and Ballistics, Hochiminh, Socialist Republic of Vietnam

OBLAST: mašinstvo
KATEGORIJA (TIP) ČLANKA: originalni naučni rad

*Sažetak:*

*Uvod/cilj: U radu je predstavljen matematički model vibracija nosača naoružanja na malom besposadnom kopnenom vozilu ukupne mase do 70 kg sa naoružanjem. Konstrukcija ovih malih vozila slična je konstrukciji većih borbenih vozila: nosač je postavljen na gusenično šasijsko postolje ili postolje sa točkovima, što omogućava elevaciju i podešavanje azimuta naoružanja, a ako je omogućeno gađanje u pokretu, vibracije šasije utiču na ugaoni položaj cevi, te je isti potrebno stabilizovati. Vibracije šasije i delova nosača naoružanja nisu poželjna pojava, a rezultati simulacije vibracija pružaju projektovanje rešenja za njihovu eliminaciju.*

*Metode: U radu su kreirani sistemi diferencijalnih jednačina koji opisuju vibracije sistema naoružanja i kretanje vozila po terenu, nakon čega je urađena simulacija vibracija u softveru u Matlab-Simulink. Dodatna ispitivanja su sprovedena u cilju merenja odstupanja ose kamere od centra mete, a rezultati eksperimenta su upoređeni sa rezultatima simulacije.*

*Rezultati: Rezultati istraživanja pokazuju da na vibracije sistema naoružanja na besposadnim kopnenim vozilima utiče mnogo faktora, kao što su profil terena, karakteristike guma, sistem vešanja, kao i ukupne dimenzije, raspored i masa komponenti. Eksperimentalni rezultati merenja stabilnosti kamere tokom praćenja mete odgovaraju rezultatima simulacije u softveru Matlab-Simulink.*

*Zaključak: Sistem matematičkih diferencijalnih jednačina besposadnog kopnenog vozila i model profila terena opisuju faktore koji utiču na vibracije sistema naoružanja tokom kretanja vozila. Matematički modeli omogućavaju promenu parametara, a time i simulaciju promena ugaonog položaja cevi u različitim uslovima unosa.*

*Ključne reči: besposadno kopneno vozilo, sistem naoružanja, stabilizacija, analiza vibracija.*

Paper received on: 5 September 2025.
Manuscript corrections submitted on: 21 November 2025.
Paper accepted for publishing on: 25 November 2025.